

Synthesis and photoluminescence study on europium ion activated titania nanoparticle

Thoudam Nando Singhi¹, Thongam Gomti Devi^{1*} and Shougaijam Dorendrajit Singh²

¹Department of Physics, North-Eastern Regional Institute of Science and Technology, Nirjuli 791109, Arunachal Pradesh, India

²Department of Physics, Manipur University, Imphal 79 003, Manipur, India

*Corresponding author, Tel: 0360-2257401; E-mail:tgdevi26@gmail.com

Received: 01 October 2016, Revised: 25 November 2016 and Accepted: 12 December 2016

DOI: 10.5185/amlett.2017.1432

www.vbripress.com/aml

Abstract

Eu³⁺ doped TiO₂ (0.2-1at. %) is synthesized successfully by non-aqueous sol-gel technique at low temperature. They are characterized structurally and optically with the used of X-ray diffraction (XRD), UV-visible spectrophotometer, Photoluminescence (PL), microscopy (SEM) and Transmission electron microscopy (TEM). The anatase to rutile phase transition is observed at 750°C and lattice distortion ratios are reduced whereas crystallites sizes are found to increase with increases of temperature. The emission spectrum under excitation at the ⁷F₀→⁵L₆ (393nm) transition of the Eu³⁺ ion shows broad emission bands arising from the ⁵D_J (J=0, 1) levels and with the emission decays lifetime varying between 0.243 and 0.375ms for samples prepared at different temperatures. The Judd-Ofelt intensity parameters Ω₂ are found in the range 6.57 - 17.14 x10⁻²⁰cm² at different concentrations and temperatures. Quantum yield of all the samples are more than 80% at different temperature. The average decay lifetime decreases with the increase of Eu³⁺ concentration. Copyright © 2017 VBRI Press.

Keywords: Titania, nanoparticle, photoluminescence, lifetime, judd-ofelt.

Introduction

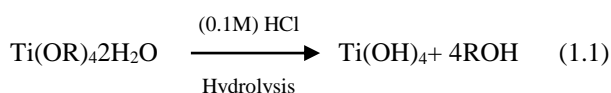
Titanium dioxide (TiO₂) is a well-known highly ionic white metal oxide n – type semiconductor material with diverse range of applications ranging from medicine, chemical to electronic industries [1-4]. It has been widely used in photocatalysis [5], photovoltaic cells [6], humidity sensors [7], Li ion batteries [8], solar cells [9], hydrogen storage [10], bio-medical engineering [11], drug delivery systems, antibacterial materials, cosmetics, sunscreens, and electronics [12], nontoxic [13], etc. It has four polymorphs in nature, including rutile (tetragonal), anatase (tetragonal) [1-2], brookite (rhombohedral) [3], and TiO₂ (B) (monoclinic). Other high pressure polymorphs have been also reported [14]. Rutile is more stable than anatase and brookite. Anatase and rutile adopted tetragonal symmetry with space group I4₁/amd and p4₂/mnm respectively, p_{bca} and c₂/m for brookite and TiO₂ (B) respectively. TiO₂ is a wide band gap semiconductor with band gap energy of 3.2 eV for the anatase crystal structure, and 3.0 eV for the rutile structure [15]. This wide band gap of TiO₂ is adequate for doping with lanthanides so that the 4f state lies within the gap which decreases the probability of nonradiative de-excitation mechanism [16]. Rutile is in the stable phase at high temperature, and is obtained in most attempts to grow TiO₂ crystals. Consequently, rutile is the most extensively investigated form of titanium dioxide, a wide-band gap semiconductor of great interest for fundamental research as well as for applications in electronic and optical devices. Nevertheless, the anatase phase can also be stabilized in the form of powders, ceramics, natural or synthetic crystals, thin films, etc. The availability of two slightly

different crystal structures for a same oxide provides a good opportunity to test our understanding of the electronic properties related to their structure. The increasing interest in anatase is demonstrated by the recent successful application of colloidal anatase in a novel photochemical solar cell [9].

As TiO₂ is a promising photocatalytic activity [17] and to enhance the photocatalytic activity, TiO₂ is doped with the rare-earth-element has become attractive to the field of material science because of their immense increase in its properties. The first requirement for the study of nanoparticle is the novel synthesis of material. The development of systematic studies for the synthesis of oxide nanoparticle is current challenge, the preparation method may be grouped in two streams based upon liquid-solid [17] and gas-solid [18] nature of the transformation. In this paper, we have used the non-aqueous sol-gel method to prepare the TiO₂ compound which is under liquid-solid transformation [19-23]. Here we used europium as representative of rare earth elements to study the effects of Eu³⁺ ion doped on the TiO₂ structure. We have prepared undoped and Eu³⁺ doped TiO₂ nanoparticle up to 1 at.% Eu³⁺ and characterized them for their structural and luminescence properties. This method is very important method for the synthesis of titania nanoparticle. The sol-gel technique is the most widely use method for being easier and inexpensive technique to prepare the materials. Furthermore, it provides a good control on chemical compositions, morphology and crystallite size of the nanomaterial. It provides compositional homogeneity that can control the structural morphology and grain size of the particles. The result of low

temperature sol-gel synthesis is amorphous in most cases and hence we require various processes to bring to crystallization state. To overcome these specific problems in hydrolytic system, sol-gel process of non-hydrolytic system have been developed. Various research groups have worked on low temperature process [24-25]. However, further study using different route and precursors is necessary to investigate new nanoparticle which have efficient properties in photocatalytic activities. Furthermore, particle size is considered as the most important parameter in nanoparticle as it has a tremendous effect on the mechanical, electronic, magnetic, and optical properties. Hence our work based on low temperature non-aqueous route is chosen for the study. The Judd-Ofelt intensity parameters Ω_2 are calculated at different concentration and at different temperatures. Low temperature synthesis of Ti nanoparticle in non-aqueous sol gel method is economically important and high efficiency method. It allows in situ functional and structural modification of the thermally unstable molecules such as biomolecules, metal-organic frameworks etc. which was considered previously impossible in crystalline titania gel. This method enables adjusting the growth of crystallites, average particle size as well as the degree of crystalline [26].

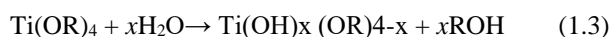
The sol-gel synthesis process involves hydrolysis and condensation reaction as two important steps. In aqueous sol-gel process, the water molecules supply the oxygen for the formation of the oxidic compound. In non - aqueous process, where intrinsically, no water is present, the question of the oxygen for the metal oxide arises. The oxygen for nanoparticle formation is provided by the solvent EtOH or titanium alkoxide [25].



where R is alkyl group. The reaction of eq. (1.1) is generally slow and does not proceed stoichiometrically to accelerate hydrolysis (0.1M) HCl is added as catalyst. The alcoholic solution will be first hydrolyzed, later polymerized and finally dehydrated, producing water as a result. The above reaction may be written as follows:



R (OH) is an aliphatic alcohol which is very quickly removed by volatilization. The above equation (1.1) does not proceed stoichiometrically and in the absence of peptizing agents, the rapid formation of partially hydrolyzed species occurs:



Equation (1.3) is followed by condensation reaction and resultant precipitation described by equation (1.4):



Experimental

Materials

The starting materials used in this study were titanium(IV) isopropoxide (TIP) $[\text{Ti}(\text{OCH}(\text{CH}_3)_2)_4]$, with

purity 98+%, Acros Organics, Newjersey, U.S.A], Europium (III) oxide $[\text{Eu}_2\text{O}_3]$, with purity 99.99%, HIMEDIA], absolute ethanol (EtOH) $[\text{C}_2\text{H}_5\text{OH}]$, with purity 99.8%, HIMEDIA], sodium hydroxide $[\text{NaOH}]$, hydrochloric acid $[\text{HCl}]$ with purity 35%, HIMEDIA] and acetone $[\text{C}_3\text{H}_6\text{O}]$, with purity 99.8%, HIMEDIA]. All the chemicals were used in a reagent grade and used without further purification.

Method

The sol-gel processing method was used for the synthesis of undoped TiO_2 and europium ion doped TiO_2 ($\text{TiO}_2 \cdot \text{Eu}^{3+}$) nanoparticle. To prepare undoped TiO_2 , 0.5ml of 0.1M HCl was dissolved in 25ml of EtOH. This mixture was labeled as A. 25ml of EtOH was added drop wise in 5ml of TIP under constant stirring using magnetic stirrer in an ice bath at 5°C. The pH of this mixture was adjusted to ~8 by using NaOH and HNO_3 and labeled as B. Mixture A was added drop wise into mixture B under constant stirring at 5°C. This mixture solution was clear and transparent then white precipitate was appeared. After 10 minutes it was turned into gel. The gel was left for ageing for two hours. Then the gel was collected for centrifugation after adding sufficient amount of EtOH and washed many times with EtOH. The result was dried in a hot air oven at 90°C for 16 hours. Finally the dried product was annealed at 220, 350, 450, 750°C for two hours. For a typical synthesis of $\text{TiO}_2 \cdot \text{Eu}^{3+}$ (0.4 at. % Eu^{3+}), 0.5ml of 0.1M HCl and 25ml of EtOH were mixed. This mixture was introduced drop wise into the vigorously stirred mixture of 5ml of TIP and 25ml of EtOH until it precipitated into milky white and pH value was adjusted at ~8 using NaOH and HNO_3 again 0.0231g of Eu_2O_3 prepared solution is added. Two necked round bottom flask of 500ml was used to remove excess HCl by evaporation and diluted with distilled water for the preparation of Eu_2O_3 prepared solution. The resulting precipitate quickly becomes gel. The gel was left for ageing for two hours. Then the gel was collected for centrifugation after adding sufficient amount of EtOH and washed many times with deionized water. The result was dried in a hot air oven at 90°C for 16 hours. Finally the dried product was annealed at 350, 450, 750°C for two hours. The similar processes were adopted for the preparation of other samples.

Characterizations

Powder X-ray diffraction (XRD) studies were performed using PAN analytical X-ray diffractometer with $\text{CuK}\alpha$ radiation ($\lambda = 1.5406 \text{ \AA}$) having tube voltage 40kV and current 30mA. XRD patterns are recorded in the angular range $20^\circ \leq 2\theta \leq 79.9^\circ$ with a step size of $\Delta 2\theta = 0.05^\circ$. The crystallite size (D) was evaluated using Debye - Scherrer relation [27]:

$$D = k\lambda / \beta \cos\theta \quad (2.1)$$

where, β is the full width at half maximum (FWHM) of the diffraction peak in radian; λ ($= 0.15406 \text{ nm}$) is the wavelength of X-ray for $\text{CuK}\alpha$; θ is the Bragg's angle measured in radian; k is a constant taken as 0.89 and known as structural constant. Average crystallite size was computed with the used of Williamson and Hall equation [28],

$$\beta \cos \theta = \lambda / \varepsilon + \eta \sin \theta \quad (2.2)$$

where, ε is the average crystallite size, η is the strain; β (measured in radian) is the FWHM of the XRD peak and θ is the Bragg's angle in radian. The phase contents of a sample can be determined from the weight fraction of rutile (W_R) generally known as Spur and Mayer [29] relation if the sample contains only anatase and rutile:

$$W_A = I_A / (0.884 I_R + I_A) \quad (2.3)$$

$$W_R = I_R / (0.884 I_A + I_R) \quad (2.4)$$

where, I_A represents the integrated intensity of the anatase (101) peak, and I_R the integrated intensity of rutile (110) peak. The weight fraction of anatase (W_A) and rutile (W_R) in anatase – rutile mixture are found to observe 0.5 and 0.56 respectively.

Transmission electron microscope (TEM) images were carried out using JEOL JEM 2100(200kV), Scanning electron microscope (SEM) images measurement were performed using FEI Quanta.PL emission spectra of prepared Eu^{3+} ion doped TiO_2 nanoparticle were measured on Perkin Elmer LS 55 Fluorescence Spectrophotometer.

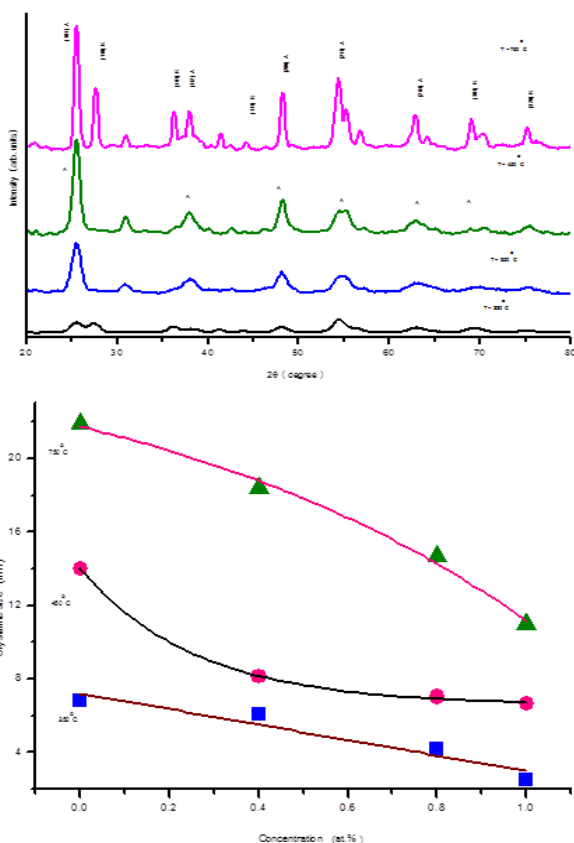


Fig. 1. (a)XRD patterns of undoped TiO_2 annealed at different temperatures ranging from 220 to 750°C. Letters represent A= anatase and R = rutile.(g)Variation of crystallites growth size of doped $\text{TiO}_2\text{:Eu}^{3+}$ (0.4, 0.8 and 1 at. %) on different concentration at different annealed temperatures.

Results and discussion

XRD study

Fig. 1(a) shows the XRD patterns of undoped TiO_2 synthesized by non-aqueous sol-gel method heat treated at 220-750°C. From XRD patterns lattice parameters are

calculated, it was found that samples prepared at 450°C exhibit tetragonal phase with space group $I4_1/amd$ (141), unit cell parameters $a = b = 3.787(1) \text{ \AA}$, $c = 9.473(6) \text{ \AA}$ and cell volume $V = 135.86 \text{ \AA}^3$. These values are comparable with JCPDS card No. 86-1157, $a = 3.783(1) \text{ \AA}$, $c = 9.497(6) \text{ \AA}$ and $V = 135.91 \text{ \AA}^3$. Cell parameters and unit cell volume increases with temperature. The sample prepared at 750°C exhibits mixed phases of $\text{TiO}_2(\text{B})$, anatase JCPDS Card No. 86-1157, rutile JCPDS Card No.78-1510. As the large mismatch of ionic radii between $\text{Eu}^{3+}(0.95 \text{ \AA})$ and $\text{Ti}^{4+}(0.74 \text{ \AA})$ unit cell volume are increasing with the increase incorporation of Eu^{3+} ions. This showed large distortion ratio (**Table 1**).

Table 1. The structure parameters of $\text{TiO}_2\text{:Eu}^{3+}$ (0, 0.4, 0.8,1 at. %) annealed at 350°C using Debye – Scherrer relation.

Eu^{3+}	450°C						
	Lattice parameters		Unit cell Volume	Cryst -allite size	Cryst -allite size	FW HM	Distor -tion
	a	c	V	D	D [33]	(β)	$\sqrt{\langle \varepsilon^2 \rangle}$
(at. %)	(Å)	(Å)	(Å^3)	(nm)	(nm)	(radian)	
0	3.77	9.11	129.5	13.4±	11.52	0.01	0.2189
	0(1)	3(6)	5	1.5	-	023	9
0.4	3.78	9.07	129.6	8.2±1.	-	0.01	0.5325
	0(1)	4(6)	5	5	-	682	3
0.5	-	-	-	-	7.59	-	-
0.8	3.78	9.40	134.2	7.0±1.	-	0.01	0.6247
	8(1)	8(6)	8	5	-	958	4
1.0	3.78	9.47	135.8	6.66±	6.54	0.02	0.6567
	7(1)	3(6)	6	1.5	-	057	0
1.5	-	-	-	-	6.52	-	-
2.0	-	-	-	-	6.49	-	-

Fig. 1(b) (shown in supplementary) shows the enlarged XRD (101) peak of undoped TiO_2 nanoparticle in the region between $2\theta = 24.5^\circ$ to 2θ at different annealed temperature (220, 350, 450, 750°C) showing increase of intensity and slight shifting of (101) peak at higher 2θ with the increase of temperature. This attributes to the enhancement of crystalline [27]. It was also found that the width of peaks decreases with the increase of annealed temperatures due to growth of crystals and construction to larger clusters. Variation of crystallites growth of undoped titania nanoparticle at different annealed temperatures has been shown in **Fig.1(c)** (shown in supplementary). It has been found that the crystallite size increases with the increase of annealed temperature. The crystal lattice distortion ratio of TiO_2 nanoparticle at different annealed temperatures is calculated by using the equation [30-32].

$$\beta^2 \cos^2 \theta = (4\lambda^2 / \pi^2 D^2) + 32(\varepsilon^2) \sin^2 \theta \quad (3.1)$$

The parameters θ , β and λ have defined already and the parameter, $\sqrt{\varepsilon^2}$ is the crystal lattice distortion ratio. According to modified Scherrer's equation (2.1) and equation (3.1), it can be deduced the lattice distortion ratio [30].

$$\sqrt{\langle \varepsilon^2 \rangle} = (\lambda / (\pi D \sin \theta)) \sqrt{(K^2 \pi^2 - 4) / 32} \quad (3.2)$$

A graph has been plotted between lattice distortions ratios of undoped titania nanoparticle determined using prefer (101) plane from XRD diffraction line broadening at different annealed temperatures (**Fig.1(d)**) (shown in supplementary). It has been found from the graph that the lattice distortion ratio is decreased with increasing the annealed temperature. This indicates that when the temperature increases, it leads to a decrease in defect concentration by decreasing in the proportion of surface atoms [32].

XRD patterns of 450°C heat treated sample of Eu^{3+} doped in TiO_2 at different concentration 0, 0.4, 0.8 and 1 at. % is shown in **Fig.1(e)**(shown in supplementary). The peaks at 25.5 degree have been chosen and compare at different doping levels (**Fig.1(f)**)(shown in supplementary). The peak position increases as the concentration of Eu^{3+} ion doped in TiO_2 increases. New peak appears on the XRD diffraction pattern as the concentration increases from 0.4 to 1 at. % doped Eu^{3+} ion. This is the indication of phase transformation from anatase to rutile. Furthermore, the variation of crystallite growth size doped with Eu^{3+} at different concentration on different annealed temperatures has been plotted (**Fig.1(g)**). We observed the crystallite size decreases as the concentration of doping increases for all temperature ranges [32,33]. It has also been observed that the crystal size increases as the temperature increases. Lattice distortion ratio of Eu^{3+} doped titania nanoparticle at different concentration on different annealed temperatures has been plotted (**Fig.1(h)**) (shown in supplementary). It has been found that distortion ratio increases as the concentration of Eu^{3+} doped is increased. It is also observed that the distortion ratio decreases as the temperature increases which is due to the decrease in defect concentration with temperature [32].

Debye – Scherrer's relation (Eqn.2.1) and Williamson-Hall equation (Eqn.2.2) have been used to calculate crystalline size. **Table 1**(shown in supporting informations) shows the lattice parameters, unit cell volume and crystallite size of nanoparticle using Debye–Scherrer's relation. **Table 2** (shown in supporting informations) shows average crystallite size and strain of the nanoparticle using Williamson-Hall equation.

TEM study

Figs. 2 (a) and **2(b)** represent TEM image of TiO_2 nanoparticle heat treated at 750°C and the Selected Area Electron Diffraction (SAED) pattern of 750°C heated sample of undoped TiO_2 respectively. The particles are found to have spherical shape with size around ~ 11nm at this temperature as can be seen from the image. The sizes obtained from TEM are in good agreement with the computed size with the use of Scherrer's relation from XRD data. Visible rings in the SAED patterns are corresponded to the (101), (004), (200) and (105) planes. The interplanar spacing d_{hkl} calculated from SAED patterns agree well with that of respective crystal planes (JCPDS Card No 86-1157).

SEM and EDX study

The SEM image and EDX of $\text{TiO}_2: \text{Eu}^{3+}$ (0.4 at. % Eu^{3+}) at 350°C are shown in **Fig.2(c)** (shown in supplementary) and **Fig. 2(d)**(shown in supplementary)

respectively. The particles are aggregated with small crystals with a broad size distribution up to 4 μm and 500 nm respectively. All the SEM images are found to observe spherical and even shape [32]. Images are not clear due to lack of sensitivity of the instrument. The EDX spectra of **Fig. 2(e)** verify the presence of Ti, O and Eu in the prepared sample. The ionic concentrations of titanium and europium of the prepared $\text{TiO}_2: \text{Eu}^{3+}$ samples are determined using EDX data. The presence of elemental Ti: Eu ratio are observed to find 94.8 and 553.6 respectively for the sample of $\text{TiO}_2: \text{Eu}^{3+}$ (0.4 at.% Eu^{3+}). A decrease in the content of titanium and an increase in the relative content of Europium are observed with the increasing nominal concentration of the doping in the samples.

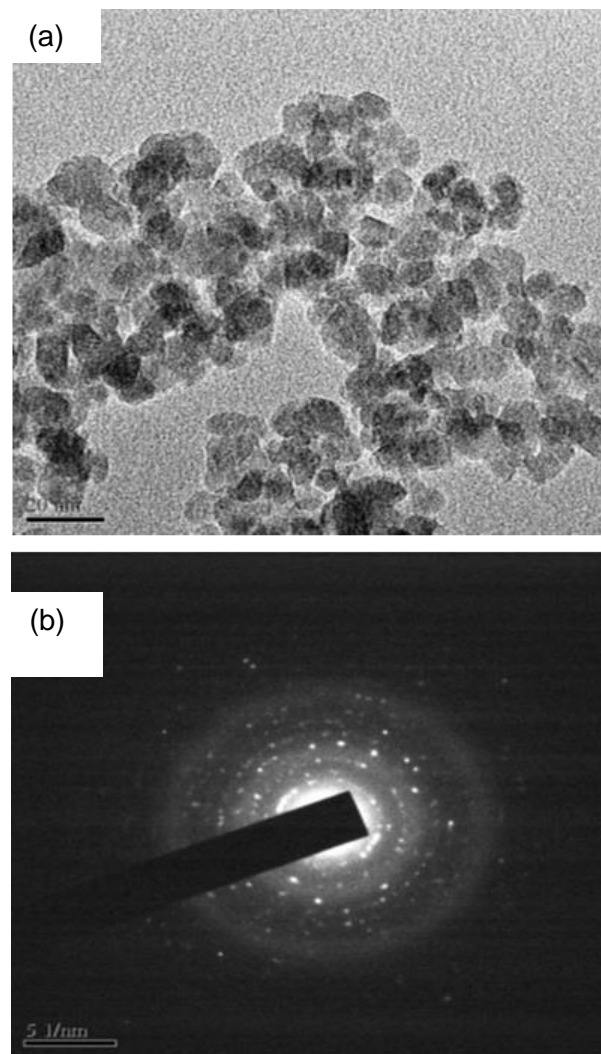


Fig. 2. (a) TEM image of TiO_2 annealed at 750°C. (b)SAED image of TiO_2 annealed at 750°C.

Luminescence study

Excitation study

Fig. 3(a) (shown in supporting information) is the representative excitation spectrum of TiO_2 doped with 0.4 at. % Eu^{3+} ion annealed at 350°C recorded at 532nm emission wavelength. The characteristic peaks of the excitation spectrum correspond to the band at 234, 250 and 393 nm that are attributed to the f-f transitions with the $\text{Eu}^{3+} 4f^6$ configuration [34]. The low shoulder peak centered at 234nm attributes host lattice absorption. The peak bands at 250-251nm correspond to Eu-O charge transfer state (CTS) caused by the electron transferred

from the oxygen 2P orbital to the empty 4f orbital of europium which may be described as ligand-to-Eu³⁺ charge transitions (LMCT) [35-36]. The inset is the enlarged region from 340–370 nm of Fig. 3(a) encompassing three sets of transition bands assigned to ⁷F₀→⁵D₄ (346nm), ⁷F₀→⁵D₄ (352 nm), ⁷F₀→⁵L₇ (360 nm) respectively. The strongest excitation peak band at 393nm attributes ⁷F₀→⁵L₆ transition. This work observed lower value of peak positions as compare to the reported value except band at 393nm [37]. Fig. 3(b) shows the change of peak position to longer wavelength (red shift) with the increase of annealing temperature from 350-750°C at 0.4 at. % particularly at the ⁷F₀→⁵L₆ transition whereas host lattice absorption region and charge transfer region are almost in the same state.

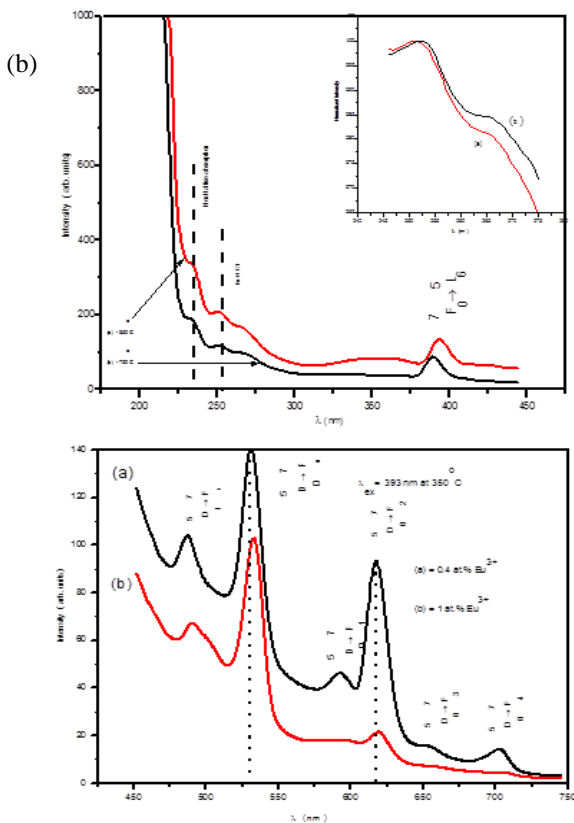


Fig. 3. (b) Excitation spectra of TiO₂:Eu³⁺ (0.4 at. % Eu³⁺) nanoparticle monitored 532 nm emission wavelength annealing at different temperature. Inset shows the enlarged view of charge region. **(c)** Photoluminescence emission peaks in the range 486-704 nm of TiO₂:Eu³⁺ (0.4 and 1 at. % Eu³⁺) nanocrystal monitored at 393 nm excitation wavelength annealed at 350°C.

the matrix and remaining emission peaks are in the visible region [36]. The weak emission peak centered at 592.8 nm assigned to ⁵D₀→⁷F₁ allowed magnetic dipole transition which is insensitive to crystal field environment and other four peaks centered at 486.2, 531, 654.5 and 704 nm assigned to the ⁵D₁→⁷F₂, ⁵D₀→⁷F₀, ⁵D₀→⁷F₃ and ⁵D₀→⁷F₄ transition is very near to the infrared region [36-38]. The electric dipole transition is much stronger than the magnetic dipole transition, suggesting that Eu³⁺ takes a low TiO₂ host lattice [39]. Emission peak intensity at 617 nm steeply decreases for sample at TiO₂:Eu³⁺ (1at. % Eu³⁺) due to concentration quenching effect. This effect comes from cross relaxation among Eu³⁺ ions which increases with decreasing distance between Eu³⁺-Eu³⁺ [40]. The electric dipole transition is depending on environment whereas magnetic dipole transition is independent of environment according to Judd- Ofelt theory [41-42]. The asymmetric ratio of PL (R₂₁) of Eu³⁺ is defined as the ratio of the intensity (I₂) of the electric dipole allowed transition (⁵D₀→⁷F₂) to the intensity (I₁) of the magnetic allowed dipole transition (⁵D₀→⁷F₁) [42]. It is very sensitive to the environment around Eu³⁺ ion. Asymmetric ratio R₂₁ is found to be 0.494 and 0.832 for TiO₂:Eu³⁺ (0.4 at. % Eu³⁺) sample annealed at 350 and 750°C respectively. The asymmetric ratio R₂₁ of TiO₂:Eu³⁺ (1 at. % Eu³⁺) sample annealed at 350°C and 750°C are found to be 0.741 and 0.781 respectively. This increase of R₂₁ at different temperatures suggests the dependence of local symmetry of Eu³⁺ [43] and lower symmetry around Eu³⁺ ions. Details are shown in Table 3. From the Commission Internationale de l'éclairage (CIE) chromacity study the colour space coordinate of 0.4 at. % Eu³⁺ doped TiO₂ sample annealed at 350°C monitored at 393 nm excitation wavelength was found to be (0.30, 0.32). Colour space coordinate of 1 at. % Eu³⁺ doped TiO₂ sample treated at the same temperature and excited wavelength was found to be (0.30, 0.33) colour space coordinate. From the calculated CIE co-ordinates (x, y) of the samples shows emission in the white region of CIE co-ordinate. These samples therefore will be good for the purpose of white light emitting devices.

Fig. 3(d) (shown in supplementary) illustrates a typical PL decay curve for ⁵D₀ emission level of doped TiO₂: Eu³⁺ (0.4 at. % Eu³⁺) annealed at 350°C. The luminescence decay is possible to the low concentration lanthanide ion in different matrices as per report [44]. The experimental decay data are fitted both in first order

Table 3. Peak intensities and position of CTS, electric and magnetic dipole transitions of Eu³⁺ in the TiO₂:Eu³⁺ samples. The ratio within the column represents peak intensity and peak position.

TiO ₂ :Eu ³⁺ (at.%)	350°C			750°C		
		Intensity			Intensity	
	⁵ D ₀ → ⁷ F ₁ (M)	⁵ D ₀ → ⁷ F ₂ (E)	E/M (R ₂₁)	⁵ D ₀ → ⁷ F ₁ (M)	⁵ D ₀ → ⁷ F ₂ (E)	E/M (R ₂₁)
0.4	45.9/591	93/617	0.494	17.8/597.3	21.4/618.8	0.832
1.0	21.6/594	28.4/617	0.741	5/588	6.4/618.5	0.781

Emission study

Fig. 3(c) shows the six characteristic PL emission peaks in the range 486-704 nm of TiO₂: Eu³⁺ (0.4 and 1 at. % Eu³⁺) nanocrystal monitored at 393nm excitation wavelength annealed at 350°C. The figure shows strong red emission band at 617 nm attributed to ⁵D₀→⁷F₂ allowed electric dipole transition indicating that the Eu³⁺ ion is located in a noncentrosymmetric position in

(mono-exponential) and second order (bi-exponential) exponential decay equations [45]:

Mono-exponential decay

$$I_t = I_0 \exp(-t/\tau) \tag{3.3}$$

where, I_t is the intensity at time t, I₀ is the intensity at time t=0 and τ is the decay life time.

Bi-exponential decay

$$I_t = I_1 \exp(-t/\tau_1) + I_2 \exp(-t/\tau_2) \quad (3.4)$$

where, I_1 and I_2 are intensities at different times and τ_1 and τ_2 is their corresponding lifetime. The average lifetime can be determined from the equation:

$$\tau_{av} = ((I_1\tau_1^2 + I_2\tau_2^2)/(I_1\tau_1 + I_2\tau_2)) \quad (3.5)$$

The average value of decay (τ_{av}) is found to be 0.35 ms (~351 μ s) of 0.4 at.% Eu^{3+} doped TiO_2 sample annealed at 350°C monitored at 352nm excited wavelength and 617nm emission wavelength, τ_1 and τ_2 are found to be 0.351ms (50% I_t) and 0.351ms (50% I_t) respectively. Former lifetime is associated with the energy transfer from Eu-O CT to Eu^{3+} and surface Eu^{3+} and latter is from the core of Eu^{3+} . A typical graph of intensity as function of time is plotted for 1 at. % Eu^{3+} doped TiO_2 annealed sample at 350°C recorded at 352nm excited wavelength and at 617 nm emission ($^5D_0 \rightarrow ^7F_2$) shown in Fig. 3(e) (shown in supplementary).

It is fitted bi-exponentially and average decay lifetime (τ_{av}) value for this sample is calculated with the use of equation (2.11). Its value is found to be 0.35ms, the same value of τ_1 and τ_2 are found to be 0.35 (50% I_t). The average decay lifetime(τ_{av}) value in the case of mono-exponential fitting is also similar to the bi-exponential fitting. The average value of decay(τ_{av}) is found to be 0.243ms (~243 μ s) for bi-exponential fitting of 1 at.% Eu^{3+} doped TiO_2 sample annealed at 350°C monitored at 352nm excited wavelength for 617nm emission ($^5D_0 \rightarrow ^7F_2$), τ_1 and τ_2 are found to be 0.243ms (50% I_t) and 0.243ms (50% I_t) respectively. For TiO_2 : Eu^{3+} (1 at. % Eu^{3+}) sample annealed at 750°C excited at 393nm for 617nm emission the average value of decay (τ_{av}) is found to be 0.375ms (~375 μ s) for bi-exponential fitting, τ_1 and τ_2 are found to be 0.407 ms (70% I_t) and 0.129 ms(29% I_t) respectively (Fig.3(f))(shown in supplementary). We have observed that the lifetime increase significantly from 243 μ s to 375 μ s as temperature increases from 350°C to 750°C. This increase in the lifetime is due to decrease in surface defects as the particle size increases with temperature [46-47]. Furthermore, it has been found from Figs. [3(d)-3(e)] (shown in supplementary) that the lifetime decreases as the concentration of doping level increases, which is of similar pattern with the decrease of luminescence intensity as Eu^{3+} concentration increases.

Evaluation of Judd-Ofelt parameters

The Judd-Ofelt (JO) theory is a powerful tool to estimate the transitions for rare-earth element, their intensity parameters, electric and magnetic dipole radiative transition probabilities. According to this theory, the JO intensity parameters describing the intensity of induced electric dipole transitions can be determined using the equation [48]

$$\frac{I_{0J}}{I_{0J}^0} = \frac{e^2 v_j^3 n(n^2 + 2)^2}{S_{md} v_1^3 9n^3} \sum \Omega_\lambda \frac{\|U_{\lambda}\|^2}{\|U_{\lambda}\|^2} \quad (3.6)$$

where, Ω_λ ($\lambda = 2, 4$) are the Judd-Ofelt intensity parameter, $\|U_\lambda\|^2$ ($\lambda= 2,4$) are the square reduced matrix elements whose values are 0.0032 and 0.0023 respectively, refractive index (n) =2.46, S_{md} is the magnetic dipole line strength

$$\frac{e^2 h^2}{16\pi^2 m^2 c^2} (\Psi J \| L + 2S \| \Psi' J')$$

where, $(\Psi J \| L + 2S \| \Psi' J')$ is the magnetic dipole matrix element, e is the electronic charge, v_j and v_1 are the transition frequencies of $^5D_0 \rightarrow ^7F_j$ and $^5D_0 \rightarrow ^7F_1$ respectively. The radiative transition probability (A_R), branching ratios (β), radiative life time(τ_R) for the $^5D_0 \rightarrow ^7F_j$ ($J=0, 1,2$) transitions of Eu^{3+} ions can be obtained using JO intensity parameter Ω_2 and Ω_4 from the following formulae.

The electric (A_{ed}) and magnetic (A_{md}) dipole radiative transition probability can be calculated from $^5D_0 \rightarrow ^7F_j$ ($J=2, 4$) and $^5D_0 \rightarrow ^7F_1$ allowed transition respectively. The expressions of A_{ed} and A_{md} are given below:

$$A_{ed} = \frac{64\pi^4 v^3}{3h(2J + 1)} \frac{n(n^2 + 2)^2}{9} S_{ed} \quad (3.7)$$

$$A_{md} = \frac{64\pi^4 v^3}{3h(2J + 1)} n^3 S_{md} \quad (3.8)$$

where, h is the Planck's constant, n is the refractive index, v is the average transition energy in cm^{-1} and $2J+1$ is the degeneracy of the initial state and S_{ed} is the electric dipole line strength given by

$$S_{ed} = e^2 \sum_{\lambda=2,4,6} \Omega_\lambda (\Psi J \| U^\lambda \| \Psi' J')^2 \quad (3.9)$$

where, e is the electronic charge, wave function Ψ and Ψ' are full intermediate-coupled functions $f^n [SL]J, U^\lambda$ are the irreducible tensor forms of the ED operator.

The total radiative transition probability (A_T) for an excited state A ($\Psi J, \Psi' J'$) and fluorescence branching ratio (β) are evaluated from the relations [48, 49]

$$A(\Psi J, \Psi' J') = A_{ed} + A_{md} \quad (3.10)$$

$$A_T = \sum_{\Psi' J'} A(\Psi J, \Psi' J') \quad (3.11)$$

$$\beta(\Psi J, \Psi' J') = \frac{A(\Psi J, \Psi' J')}{A_T(\Psi J, \Psi' J')} \quad (3.12)$$

The rate of depopulation of an excited state is defined by the radiative lifetime(τ_R)

$$\tau_R(\Psi J, \Psi' J') = \frac{1}{A_T(\Psi J, \Psi' J')} \quad (3.13)$$

The cross-section of stimulated emission ($\sigma(\lambda_p)$, between the state $|\Psi J\rangle$ and $|\Psi' J'\rangle$) is related to the radiative transition probability A as

$$\sigma_{(\lambda_p)}(\Psi J, \Psi' J') = \frac{\lambda_p^4 A(\Psi J, \Psi' J')}{8\pi c n^2 \Delta\lambda_{eff}} \quad (3.14)$$

where c is the speed of light, λ_p the peak wavelength and $\Delta\lambda_{eff}$ is the effective bandwidth of the emission peak

found by dividing the integrated area of the emission band by its average height.

Table (4-7) (shown in supporting information) list the Judd-Ofelt intensity parameters, radiation probabilities, branching ratios, radiation life time and stimulated emission cross-section for each sample concentration at different temperatures. The branching ratios for the $^5D_0 \rightarrow ^7F_2$ emission transition more than 90% at 0.4 and 1at. % Eu^{3+} doped samples. The branching ratios are found decreased as the temperature increases- the branching ratio for 0.4 at. % at 350°C is found to be 96.2% as compare to 91.78% at 750°C. We are observing the same pattern at 1at. % Eu^{3+} doped concentration. However, we are getting branching ratios of these transition above 90% for all europium doped concentrations. Hence this is the most sensitive transition. The radiative lifetime for 5D_0 levels are observed at 0.175 ms and 0.382 ms for 0.4 at. % Eu^{3+} doped samples at temperature 350°C and 750°C respectively. Similarly, the radiative lifetime of $\text{TiO}_2:\text{Eu}^{3+}$ (1at. % Eu^{3+}) sample are observed to increase at temperature 350°C and 750°C respectively. This increase of lifetime with the increase of temperature is due to decrease in surface defects as the particle size increases with temperature [46-47]. This calculated value of radiative lifetime is comparable with the experimental data. The luminescence quantum yield(η) are observed at 93.94% and 94.71% for 0.4 at.% Eu^{3+} doped TiO_2 samples at temperature 350°C and 750°C respectively. However, we are getting η value as 90.27% and 88.47% for 1.0 at. % Eu^{3+} doped TiO_2 at different temperatures. The decrease in quantum efficiency is the beginning of material structural disorder. In our study, systematic variation is observed to decrease in the values of η as the concentration increases. In general intensity increases with increase in do pant concentration then decreases due to concentration quenching. This indicates optimum value of doping concentration is less than 1 at.% Eu^{3+} in our case. The asymmetry ratios are obtained at 0.494 and 0.832 in 0.4 at. % Eu^{3+} doped TiO_2 samples at temperature 350°C and 750°C respectively. This increase of asymmetric ratio at different temperatures suggests the dependence of local symmetry of Eu^{3+} . The stimulated emission cross-sections, $\sigma(\lambda_p)$ for $^5D_0 \rightarrow ^7F_2$ transitions are observed at $125.86 \times 10^{-22} \text{cm}^2$ and $11.031 \times 10^{-22} \text{cm}^2$ for 0.4 at. % Eu^{3+} doped TiO_2 samples at temperature 350°C and 750°C respectively. Similar patterns are observed in 1at. % Eu^{3+} doped TiO_2 . It increases with the increase of transition energy (λ_p) and decreases with the increase of temperature.

Conclusion

The Eu^{3+} ion doped and undoped titania nanocrystals were synthesized by non - aqueous sol-gel technique at low temperature which were characterized by using (XRD), PL and TEM respectively. We could get the crystallite size of the range of 2-11 nm using Williamson-Hall equation which is consistent with the TEM result. In photoluminescence study, we have observed that the lifetime increases significantly as the temperature increases. Furthermore, the value of lifetime is found to decrease as the concentration of doping level increases and its value increases with the increase in annealing temperatures. The presence of

anatase and rutile phases and their transition states from anatase to rutile are also confirmed by XRD data. The radiative life time was calculated using Judd-Ofelt theory and the calculated value of radiative lifetime is found comparable with the experimental life time value obtained from emission spectra.

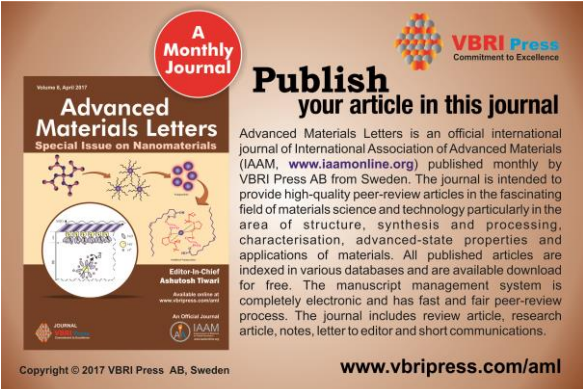
Acknowledgements

The authors are grateful to FIST- DST, Delhi for instrumentation facilities in the Department of Physics, NERIST, Arunachal Pradesh, India.

References

- Tennakone, K.; Kumara, G. R. R. A.; Kottegoda, L. R. M.; Perera, V. P. S.; Weerasundara, P. S. R. S.; *J. Photochem. Photobiol.*, **1998**,117, 137.
- Long, H.;Chen, A.; Yang, G.; Li, Y.; Lu, P.; *Thin Solid Films*, **2009**, S17, 5601.
- Li, Q.; Mahendra, S.; Lyon, D.Y.; Brunet, L.; Liga, M. V.; Li, D.; Alvarez, P. J. J.; *Water Res.*, **2008**, 42, 4591.
- Deng, D.; Kim, G. M.; Li, J. Y.; Cho, K. J.; *Energy Environ. Sci.*, **2009**, 2, 817.
- Wang, G.; Wang, H.; Ling, Y.; Tang, Y.; Yang, X.; Fitzmorris, R. C.; Wang, C.; Zhang, J. Z.; Li, Y.; *Nano.Lett.*,**2011**,11, 3026.
- Chen, X.; Liu, Y.; Yu, P. Y.; Mao, S. S.; *Nanocrystals Science*, **2011**, 331, 746.
- Zhang, Y.; Fu, W.; Yang, H.; Qi, Q.; Zeng, Y.; Zhang, T.; Ge, R.; *Appl. Surf. Sci.*,**2008**,254, 5545.
- Zukalova, M.; Kalbac, M.; Kavan, L.; Exnar, I.; Graetzel, M.; *Chem. Mater.*,**2005**,17, 1248.
- Xu, C.; Shin, P. H.; Cao, L.; Wu, J.; Gao, D.; *Chem. Mater.*, **2010**,22, 143.
- Bavykin, D.V.; Lapkin, A. A.; Plucinski, P. K.; Friedrich, J. M.; Walsh, F. C.;*J. Phys.Chem. B*,**2005**,109 [41], 19422.
- Das, G.K.; Yang-Tan, T.T.; *J. Phys. Chem.*,**2008**,112, 11211.
- Hongbo, S.; Magaye, R.; Castranova, V.; Zhao, J.; *Particle and Fibre Toxicology*,**2013**,10, 15.
- Liu, K.; Lin, X.; Zhao, J.; *Int.J.Nanomedicine*,**2013**,8, 2509.
- Muscat, J.; Swamy, V.; Harrison, N. M.; *Phys.Rev.B*,**2002**,65, 224112.
- Mills, A.; Hunte, S. L.;*J. Photochemistry and photobiology A: Chemistry*,**1997**,108, 1.
- Kenyon, A. J.; *Prog. Quant. Electron*,**2002**,26, 225.
- Xu, Z.; Yang, Q.; Xie, Ch.; Yan, W.; Du, Y.; Gao, Zh.; Zhang, J.; *J. Mater. Science*,**2005**,40, 1539.
- Rodríguez, J. A.; Fernandez-Garcia, M.(Eds.); *Synthesis, Props. and Application of oxide Nanomaterials*; Wiley:N.J, **2007**, p.81
- Zeng, G.; Ding, Z. J.; Zhang, Z. M.; *J. Lumin.*,**2006**, 118, 301.
- Zeng, Q. G.; Zhang, Z. M.; Ding, Z. J.; Wang, Y.; Sheng, Y. Q.; *Script. Mater.*,**2007**,57, 897.
- Saif, M.; Abdel-Mottaleb, M. S. A.; *Inorg. Chim. Acta*, **2007**,360, 2863.
- Stengl, V.; Bakardjieva, S.; Murafa, N.; *Mater. Chem. Phys.* **2009**, 114, 217.
- Rocha, L. A.; Molina, E. F.; Ciuffi, K. J.; Calefi, P. S.; Nassar, E. J.; *Mater. Chem. Phys.*,**2007**,101, 238.
- Ani, J. K.; Savithri, S.; Surender, G. D.; *Aerosol and Air Quality Research*, **2005**,5, 1.
- Niederberger, M.; *Acc. Chem. Res.*,**2007**,40, 793.
- Alexandr, V. V.; Vladimir, V. V.; *RSC Adv.*,**2014**,4, 45903
DOI:10.1039/c4ra04454a
- Chen, L.; Chen, K.; Hu, S.; Liu, R.; *J. Mater. Chem.*,**2011**,21, 3677.
- Williamson, G. K.; Hall, W.; *Acta Metallurgica*, **1953**,1, 22.

29. Spurr, R. A.; Myers, H.; Analytical chemistry, 1957, 29, 760.
Gao, S.; Pang, L.; Che, H.; Zhou, X.; *China Particuology*, **2004**, *2*, 177.
30. Ashutosh Tiwari, Anthony PF Turner (Eds), Biosensors Nanotechnology, John Wiley & Sons, USA, **2014**.
31. Gaber, A.; Abdel-Rahim, M. A.; Abdel-Latif, A. Y.; Abdel-Salam, M. N.; *Int. J. Electrochem. Sci.*, **2014**, *9*, 81.
32. Pal, M.; Pal, U.; Gracia, J. M.; Jimenez, Y., Pérez-Rodríguez, F.; *Nano Res. Lett.*, **2012**, *7*, 1.
DOI: [10.1186/1556-276X-7-1](https://doi.org/10.1186/1556-276X-7-1)
33. Chen, D.; Zhu, Q.; Zhijin, Lv.; Deng, X.; Zhou, F.; Deng, Y.; *Mater. Res. Bull.*, **2012**, *47*, 3129.
DOI: [10.1016/j.materresbull.2012.08.021](https://doi.org/10.1016/j.materresbull.2012.08.021)
34. Liu, B.; Wen, L.; Zhao, X.; *Materials Chemistry and Physics*, **2007**, *106*, 350.
35. Yun, M.; Zhang, W.; Xia, S.; Krupa, J. C.; *J. Lum.*, **1996**, *68*, 335.
36. Atul Tiwari, Ashutosh Tiwari (Eds), Bioengineered Nanomaterials, CRC Press, USA, **2013**.
37. Podhorodecki, A.; Zatoryb, G.; Sitarek, P.; Misiewicz, J.; Kaczmarek, D.; Domaradzki, J.; Borkowska, A.; Prociow, E. L.; *Thin Solid Films*, **2009**, *517*, 6331.
DOI: [10.1016/j.tsf.2009.02.080](https://doi.org/10.1016/j.tsf.2009.02.080)
38. Conde-Gallardo, A.; Garcia-Rocha, M.; Hamandez-Calderon, I.; Palom Merino, R.; *Appl. Phys. Lett.*, **2001**, *78*, 3436.
39. Borlaf, M.; Colomer, M. T.; Moreno, R.; de Andres, A.; *J. Am. Ceram. Soc.*, **2015**, *98*, 338.
40. Schmechel, R.; Kenndy, M.; Seggern, H. V.; Winkler, H.; Kolbe, M.; Fischer, R. A.; Li, X.; Benker, A.; Winterer, M.; Hahn, H.; *J. Appl. Phys.*, **2001**, *89*, 1679.
41. Judd, B. R.; Physical Review, 1962, 127, 750.
DOI: [10.1103/PhysRev.127.750](https://doi.org/10.1103/PhysRev.127.750)
42. Ofelt, G. S.; *J. Chem. and Phys.*, **1962**, *37*, 511.
DOI: [10.1063/1.1701366](https://doi.org/10.1063/1.1701366)
43. Smits, K.; Grigorjeva, L.; Millers, D.; Sarakovskis, A.; Opalinska, A.; Fidelus, J. D.; *Lojkowski, W.; Optical Materials*, **2010**, *32*, 827.
44. Moon, B. K.; Kwon, I. M.; Jeong, J. H.; Kim, C. K.; Yi, S. S.; Kim, P. S.; Choi, H.; Kim, J. H.; *J. Lumin.*, **2007**, *122/123*, 855.
45. Yu, M.; Lin, J.; Fang, J.; *Chem. Mater.*, 2004, 17, 1783.
46. Ashutosh Tiwari, Atul Tiwari (Eds), In the Nanomaterials in Drug Delivery, Imaging, and Tissue Engineering, John Wiley & Sons, USA, **2013**.
47. Singh, N. S.; Ningthoujam, R. S.; Luwang, M. N.; Singh, S. D.; Vatsa, R. K.; *J. Appl. Phys.*, **2009**, *105*, 064303.
48. Barve, R.A.; Suriyamurthy, N.; Panigrahi, B.S.; Venkatraman, B.; *Physica B*, **2015**, *475*, 156.
49. Munirathnam, K.; Dillip, G. R; Raju Prasad, D. B.; Joo, S.W.; Dhoble, S.J.; Nagabhusana, B.M.; Krishna Hari, R.; Ramesh, K.P.; PerumalVaradharaj, S.; Prakashbabu, D.; *Appl. Phys. A*, **2015**, *120*, 1615.



A Monthly Journal

Publish your article in this journal

Advanced Materials Letters is an official international journal of International Association of Advanced Materials (IAAM, www.iaamonline.org) published monthly by VBRI Press AB from Sweden. The journal is intended to provide high-quality peer-review articles in the fascinating field of materials science and technology particularly in the area of structure, synthesis and processing, characterisation, advanced-state properties and applications of materials. All published articles are indexed in various databases and are available download for free. The manuscript management system is completely electronic and has fast and fair peer-review process. The journal includes review article, research article, notes, letter to editor and short communications.

Editor-in-Chief: Ashutosh Tiwari

www.vbripress.com/aml

Copyright © 2017 VBRI Press AB, Sweden

Supplementary information

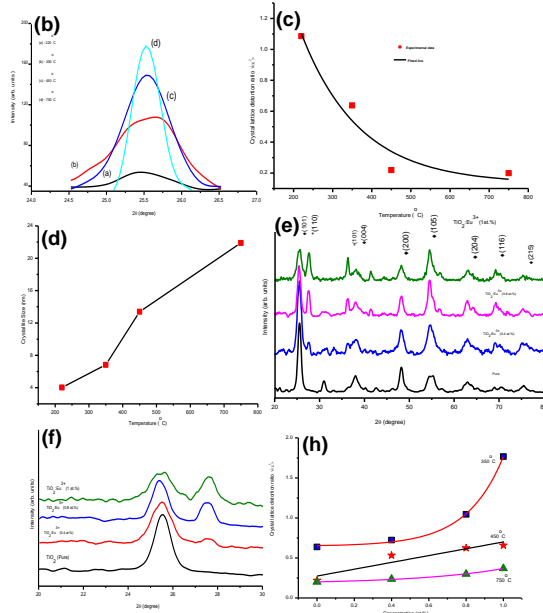


Fig. 1. (b) XRD patterns of enlarged view of Fig .1(a) ranging from 24-27 (degree) for undoped TiO₂ annealed at different temperature (220,350,450,750°C). 1(c) Variation of crystallites growth size of undoped doped TiO₂ at different annealed temperatures. (d) Variation of lattice distortion ratios of undoped titania nanoparticle at different annealed temperatures. (e) XRD patterns of undoped TiO₂ and doped TiO₂:Eu³⁺(0.4,0.8,1 at. %) nanoparticle. Symbols represent diamond = anatase and asterisk = rutile (f) XRD patterns of enlarged view of Fig .1(e) ranging from 24-30 (degree) for undoped TiO₂ and doped TiO₂:Eu³⁺(0.4,0.8 and 1 at. %). (h) Variation of crystallites growth size of doped TiO₂:Eu³⁺ on different concentration (0.4,0.8 and 1 at. %) at different annealed temperatures.

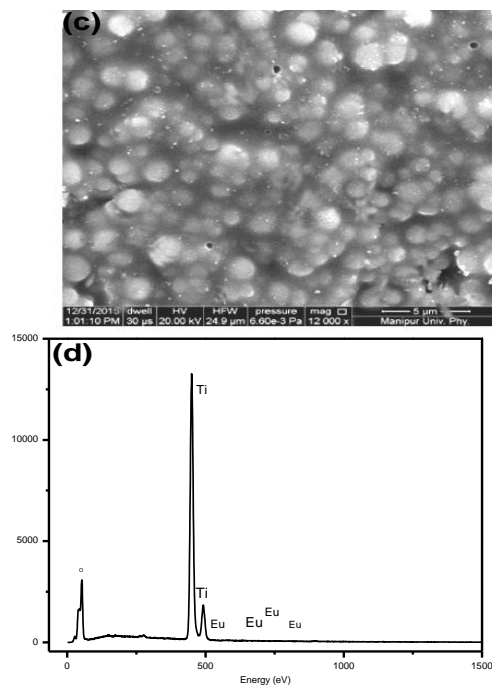


Fig. 2. (c) SEM image of TiO₂ :Eu³⁺ (0.4 at.% Eu³⁺) annealed at 750°C (d) EDX spectrum of TiO₂ annealed at 750°C.

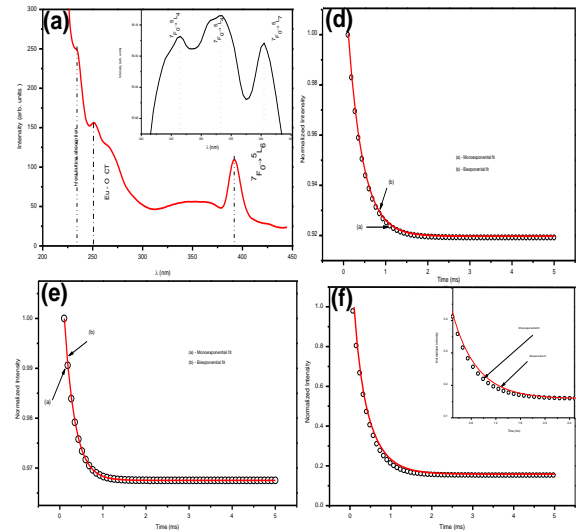


Fig. 3. (a)Excitation spectrum of TiO₂ :Eu³⁺(0.4 at.% Eu³⁺) annealed at 350°C recorded at 532 nm emission wavelength and the inset shows the enlarged region around 7F₀ → 5L₆ transition. (d) PL decay curve for 5D₀ emission level of TiO₂:Eu³⁺ (0.4 at.% Eu³⁺) annealed at 350°C recorded at 352 nm excited wavelength and at 617 nm emission (5D₀ → 7F₂). (e) PL decay curve of TiO₂ :Eu³⁺ (1.0 at. % Eu³⁺) annealed at 350°C recorded at 393 nm excited wavelength and at 617 nm emission (5D₀ → 7F₂).

Table 2. The structure parameters of TiO₂:Eu³⁺ (0, 0.4, 0.8,1 at. %) annealed at 350°C using Williamson-Hall equation.

TiO ₂ :Eu ³⁺ (at.%)	Crystallite Size(D) (nm)	Strain(η)
0.0	7	1.14x10 ⁻²
0.4	6	2.23x10 ⁻²
0.8	4	2.46x10 ⁻²
1.0	3	8.10x10 ⁻²

Table 4. Calculated radiative parameters of TiO₂:Eu³⁺ (0.4 at.% Eu³⁺) at different annealing temperature.

Temp.	Eu(at.%)	Transition	λ (nm)	Area	$A_{md}(S^{-1})$	$A_{ed}(S^{-1})$	$A_T(S^{-1})$	τ_R (ms)	τ_{NR} (ms)	β (%)	η (%)
350°C	0.4	⁵ D ₀ ? ⁷ F ₁	592.5	75.26	215.37	—	2677.39	0.373	172.42	3.77	93.94
		⁵ D ₀ ? ⁷ F ₂	618	712.31	—	2462.02	—	—	—	96.2	—
		⁵ D ₀ ? ⁷ F ₄	703	99.404	—	—	—	—	—	—	—
750°C	0.4	⁵ D ₀ ? ⁷ F ₁	593	8.209	215.35	—	2619.33	0.382	146.16	8.22	94.71
		⁵ D ₀ ? ⁷ F ₂	620	90.705	—	2403.98	—	—	—	91.78	—
		⁵ D ₀ ? ⁷ F ₄	709.5	0.6684	—	—	—	—	—	—	—

Table 5. Calculated radiative parameters of TiO₂:Eu³⁺ (1 at.% Eu³⁺) at different annealing temperature.

Temp.	Eu(at.%)	Transition	λ (nm)	Area	$A_{md}(S^{-1})$	$A_{ed}(S^{-1})$	$A_T(S^{-1})$	τ_R (ms)	τ_{NR} (ms)	β (%)	η (%)
350°C	1.0	⁵ D ₀ → ⁷ F ₁	592.5	55.872	215.896	-	3714.966	0.2692	400.27	5.81	90.27
		⁵ D ₀ → ⁷ F ₂	618	771.523	-	3499.07	-	-	-	94.18	-
		⁵ D ₀ → ⁷ F ₄	703	91.049	-	-	-	-	-	-	-
750°C	1.0	⁵ D ₀ → ⁷ F ₁	588	0.82415	220.89	-	2358	0.4241	307.25	9.367	88.47
		⁵ D ₀ → ⁷ F ₂	615.5	4.31576	-	2137.11	-	-	-	90.63	-
		⁵ D ₀ → ⁷ F ₄	709.5	0.6684	-	-	-	-	-	-	-

Table 6. Calculated Judd-Ofelt intensity parameters of TiO₂:Eu³⁺ (0.4 at.% Eu³⁺) at different annealing temperature.

Temp.	Eu(at.%)	Transition	λ (nm)	$\Omega_2(10^{-20}) \text{ cm}^2$	$\Omega_4(10^{-20}) \text{ cm}^2$	Asymmetry ratio	β (%)	$\sigma(10^{-22}) \text{ cm}^2$
350°C	0.4	⁵ D ₀ → ⁷ F ₁	592.5	11.75	3.35	0.494	3.77	-
		⁵ D ₀ → ⁷ F ₂	617	-	-	-	96.2	125.86
		⁵ D ₀ → ⁷ F ₄	703	-	-	-	-	197.14
750°C	0.4	⁵ D ₀ → ⁷ F ₁	593	13.81	0.212	0.832	8.22	-
		⁵ D ₀ → ⁷ F ₂	620	-	-	-	91.78	11.031
		⁵ D ₀ → ⁷ F ₄	709.5	-	-	-	-	21.584

Table 7. Calculated Judd-Ofelt intensity parameters of $\text{TiO}_2:\text{Eu}^{3+}$ (1.0 at. % Eu^{3+}) at different annealing temperature.

Temp.	Eu(at.%)	Transition	$\lambda(\text{nm})$	$\Omega_2(10^{-20})\text{cm}^2$	$\Omega_4(10^{-20})\text{cm}^2$	Asymmetry ratio	$\beta(\%)$	$\sigma(10^{-22})\text{cm}^2$
350°C	1	$^5\text{D}_0 \rightarrow ^7\text{F}_1$	592.5	17.1414	4.1428	0.741	5.81	-
		$^5\text{D}_0 \rightarrow ^7\text{F}_2$	618	-	-	-	94.2	79.47
		$^5\text{D}_0 \rightarrow ^7\text{F}_4$	703	-	-	-	-	124.99
750°C	1	$^5\text{D}_0 \rightarrow ^7\text{F}_1$	588	6.57	7.752	0.781	9.367	-
		$^5\text{D}_0 \rightarrow ^7\text{F}_2$	615.5	-	-	-	90.63	44.015
		$^5\text{D}_0 \rightarrow ^7\text{F}_4$	709.5	-	-	-	-	-